

Anisotropic magnetic response of a chiral conducting film

D. P. Druist,¹ E. G. Gwinn,¹ K. D. Maranowski,² and A. C. Gossard²

¹Physics Department, UCSB, Santa Barbara, California 93106, USA

²Materials Department, UCSB, Santa Barbara, California 93106, USA

(Received 6 May 2003; published 13 August 2003)

We use tilted magnetic fields to study the magnetoresistance of the chiral sheath of edge states that transports charge through GaAs/AlGaAs multilayers in the integer quantum Hall regime. The magnetic field component perpendicular to the layer planes \mathbf{B}_z establishes the quantum Hall state, while the in-plane field $\mathbf{B}_{\text{plane}}$ is either perpendicular or parallel to the edge-state sheath on a given mesa wall. We find orientation-dependent response of the sheath's vertical conductivity to $\mathbf{B}_{\text{plane}}$, with lower conductivity for fields that link flux through the sheath.

DOI: 10.1103/PhysRevB.68.075305

PACS number(s): 78.66.-w, 73.61.Ey, 75.47.De

Electronic trajectories in conductors largely determine the response of the conductivity to applied magnetic fields. In conventional conducting films electrons move in random two-dimensional walks. Perpendicular fields link magnetic flux through closed time-reversed paths and destroy their constructive quantum interference, typically increasing the conductivity. Here we investigate experimentally the conductivity in applied magnetic fields of a conducting film in which electrons execute random walks in only one direction, and flow one way in the perpendicular direction. This special conducting film is the chiral sheath of edge states that forms at the walls of semiconductor multilayers in the integer quantum Hall (QH) regime.¹⁻⁷ We find that the response of the sheath's conductivity to applied fields differs qualitatively from that of conventional conducting films.

Figure 1(a) sketches the system. The one-dimensional edge states that encircle each quantum well of the GaAs/AlGaAs multilayer couple by tunneling to form the chiral sheath. We use the field component perpendicular to the layers \mathbf{B}_z to create the edge-state sheath. This surface conducting phase dominates charge transport only over ranges of \mathbf{B}_z that produce the quantum Hall effect for transport parallel to the layer planes, while the entire volume of the sample contributes to transport over fields in the transitional regions between quantum Hall (QH) states, as demonstrated previously.¹ Tilting the samples relative to the field axis creates an additional field $\mathbf{B}_{\text{plane}}$ in the layer planes. The experimental geometry orients $\mathbf{B}_{\text{plane}}$ either perpendicular or parallel to the edge-state sheath on the sidewalls of the rectangular sample mesas [Fig. 1(b)]. By comparing the conductances of different mesas we determine the conductivity σ_{\perp} of the chiral sheath perpendicular to $\mathbf{B}_{\text{plane}}$ and the conductivity σ_{\parallel} of the chiral sheath parallel to $\mathbf{B}_{\text{plane}}$.

In vertical transport experiments, QH states appear as deep minima in the conductance G perpendicular to the layers. Figure 1(d) shows a semilog plot of G versus B_z for several tilt angles θ . We focus on the QH state indicated by the hatched area labeled $\nu=1$. Earlier in-plane transport experiments indicated that this state, which runs from $B_z \sim 8$ T to $B_z \sim 13$ T, corresponds to occupation of the lowest spin-split Landau band of the multilayer.¹

Previous studies²⁻⁴ showed that arbitrarily oriented $\mathbf{B}_{\text{plane}}$ can alter the conductivity of the chiral sheath through the

strength of interlayer tunneling²⁻⁴ t^2 . Studies of a similar GaAs/AlGaAs multilayer⁴ showed that the reduction of G by $\mathbf{B}_{\text{plane}}$ was consistent with theoretical calculations for bulk tunneling between weakly coupled quantum wells,⁸ which predicted $G \sim t^2$ and

$$t^2 = t_0^2 \exp(-2[B_{\text{plane}}/B^*]^2) \quad (1)$$

for the $\nu=1$ quantum Hall state. In Eq. (1), t_0 is the tunneling matrix element at zero field, $B^* = 2B_z l_z/d$, $l_z = (\hbar/2\pi e B_z)^{1/2}$ is the magnetic length corresponding to B_z , and d is the layer spacing.

Previous studies by others of GaAs/AlGaAs multilayers⁴ did not investigate effects of changing the orientation of $\mathbf{B}_{\text{plane}}$ with respect to the chiral sheath. Here we use an experimental geometry that allows us to reveal anisotropic response of the conductivity to $\mathbf{B}_{\text{plane}}$.

Theory predicts⁷ different vertical conductivities for regions of the edge-state sheath that are perpendicular or parallel to the in-plane field. The physical origin for this predicted anisotropy is the Lorentz force that $\mathbf{B}_{\text{plane}}$ exerts on edge trajectories. Because the chiral drift velocity in an edge state is parallel to the edge, regions of the edge sheath that are perpendicular to the in-plane field $\mathbf{B}_{\text{plane}}$ experience an edge Lorentz force, while regions of the edge sheath that are parallel to $\mathbf{B}_{\text{plane}}$ do not. Theory predicts that this leads to a Drude dependence of the ratio of the perpendicular and parallel conductivities on the magnitude B_{plane} of the in-plane field

$$\sigma_{\perp}/\sigma_{\parallel} = [1 + (B_{\text{plane}}/B_0)^2]^{-1}, \quad (2)$$

where B_0 is a characteristic field. The conductivity σ_{\parallel} depends on the chiral sheath parameters as^{6,7}

$$\sigma_{\parallel} = (e^2/h)t^2 l_{\text{el}} d / (\hbar v_{\text{edge}})^2. \quad (3)$$

Here, d is the layer spacing and v_{edge} is the chiral drift velocity in an edge state.

The edge-sheath conductivities in Eqs. (2) and (3) depend on an edge elastic scattering length l_{el} . This length scale is the distance electrons in adjacent edge states must travel to accumulate a phase difference of unit magnitude.⁷ The characteristic field B_0 for the decay of $\sigma_{\perp}/\sigma_{\parallel}$ in Eq. (2) is the magnitude of the $\mathbf{B}_{\text{plane}}$ that links a flux quantum through an

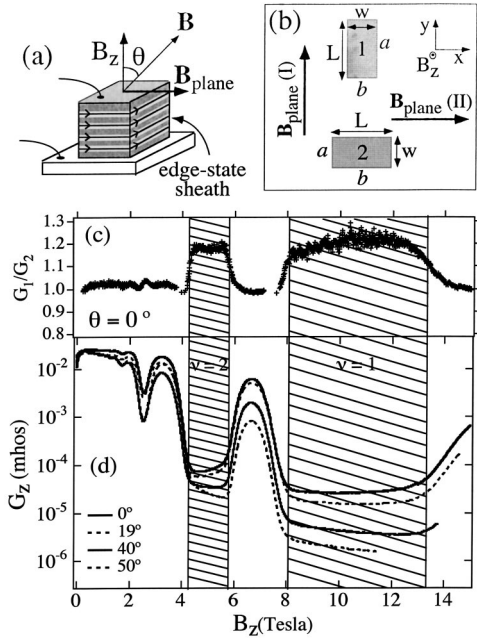


FIG. 1. Sample geometry and measured conductance. (a) Schematic of a vertical transport mesa. Current flows perpendicular to the layers of a GaAs/AlGaAs multiple-quantum-well structure. The field perpendicular to the layers \mathbf{B}_z establishes the quantized Hall states. In these states, the bulk is localized and the chiral edge-state network carries the transport current. The lines with arrows represent the edge states that encircle the GaAs quantum wells. These edge states couple to form the chiral surface sheath, which has charge flowing in one direction around the perimeter. (b) Schematic top view of the sample mesas, which have identical dimensions. The conductance G perpendicular to the layers was measured in two configurations: in I(II), the in-plane field $\mathbf{B}_{\text{plane}}$ was parallel to crystal face $a(b)$. (c) Ratio G_1/G_2 of the conductances of mesas 1 and 2, for no tilt ($\mathbf{B}_{\text{plane}}=0$). Hatched regions mark the ranges of \mathbf{B}_z that correspond to the $\nu=1$ and $\nu=2$ per layer QH states. (d) Conductance of mesa 1, measured in configuration I, versus the vertical component of the magnetic field \mathbf{B}_z for a number of tilt angles. As the tilt angle, and hence $\mathbf{B}_{\text{plane}}$, increases, the conductance decreases.

area dl_{el} on the edge sheath: $B_0 = h/(edl_{\text{el}})$. Thus, although l_{el} is undefined in single-layer quantum Hall systems, Eqs. (2) and (3) show that it is an important parameter of the chiral sheath that determines the anisotropy in its response to $\mathbf{B}_{\text{plane}}$.⁷

The model⁷ that yields Eq. (2) assumes that transport on the sheath is at least partially coherent. For incoherent transport, the edge-sheath conductivity should be unaffected by flux through the chiral sheath,⁷ yielding a constant ratio $\sigma_{\perp}/\sigma_{\parallel}$.

We study a GaAs/Al_{0.1}Ga_{0.9}As multilayer¹ grown by molecular beam epitaxy with 50 periods of 150 Å GaAs quantum wells that alternate with 150 Å barriers. Thus the period d of the multilayer is 300 Å and the total height of the multilayer is $H = 1.5 \mu\text{m}$. The multilayer is Si δ doped at the barrier centers to a per-layer sheet density of $2.3 \times 10^{11} \text{ cm}^{-2}$. We pattern this material into $W = 150 \mu\text{m}$ by $L = 300 \mu\text{m}$ mesas, oriented at 90° to one another, as

sketched in Fig. 1(b). The mesa walls were closely aligned with the GaAs cleavage planes, which we refer to as faces a and b , for simplicity. To achieve smooth walls, we defined the top AuNiGe contact metallization using electron-beam lithography. After lift off, this metallization served as an etch mask for a SiCl_4 reactive ion etch, which leaves nearly vertical mesa walls. Subsequent deposition of bottom contacts and annealing yielded Ohmic contacts. Scanning electron micrograph (SEM) images⁹ show that mesa wall roughness in these samples is on scales of ~ 1000 Å and smaller.

All data shown here were taken at a temperature of 100 mK, where in QH states, in-plane transport is well quantized and vertical transport through the bulk is negligible.¹ Thus the conductances measured in QH states sample the properties of the chiral sheath. We made the measurements in a dilution refrigerator with room-temperature filtering and coax sample lines to the low-temperature filter stages. To vary the angle the magnetic field makes with the planes of the multilayer, we mounted the sample on an *in situ* rotator platform with 1° angle reproducibility. Care was taken to exclude noise via proper grounding and filtering, and to keep excitation small ($V < 10 \mu\text{V}$) to avoid electron heating. The field was swept to 18 T with the superlattice planes at various angles θ to the field direction. The low-temperature apparatus, the filter rig, and the measurement technique are described in detail in a preliminary report.⁹

We first examine the no tilt ($\theta=0$) behavior of the conductances G_1 and G_2 of mesa 1 and mesa 2. Figure 1(c) plots the ratio G_1/G_2 of conductances measured in the same thermal cycle. For comparison, the solid trace in Fig. 1(d) is the conductance G_1 of mesa 1, also at $\theta=0$. In QH states, which are the deep minima in G in Fig. 1(d), the bulk is frozen out, so transport is along the chiral sheath. For field ranges outside the QH states, where bulk transport dominates, Fig. 1(c) shows $G_1 \approx G_2$, indicating that the bulk properties of the mesas are the same. However, within QH states $G_1/G_2 \approx 1.2$ at $\theta=0$. These results were consistent between thermal cycles. Across quantum Hall states, thermal cycling between 100 mK and 300 K typically produced changes in mean conductance of $\sim 2\%$ in these samples.

If the conductivities of the portions of the chiral sheath on type a and b crystal faces were identical, G_1 would equal G_2 for the untilted mesas, since their dimensions are identical. The difference in G_1 and G_2 corresponds to a conductivity ratio $\sigma_a/\sigma_b \approx 1.8$ on type a and type b crystal faces, somewhat larger than typical in-plane transport anisotropies found in Hall bars oriented at right angles on GaAs/AlGaAs quantum wells. Differences in v_{edge} , l_{el} , or t on the different crystal faces, or differences in microscopic roughness, could perhaps account for this behavior.

To analyze the conductance data in tilted fields, we assume that opposite mesa walls, etched along the same crystal face, have the same behavior. Then there are four chiral sheath conductivities in the QH states: $\sigma_{a,\parallel}$ on type a faces, for parallel $\mathbf{B}_{\text{plane}}$; $\sigma_{a,\perp}$ on type a faces, for perpendicular $\mathbf{B}_{\text{plane}}$; and $\sigma_{b,\parallel}$ and $\sigma_{b,\perp}$ on type b faces. To extract these four conductivities, we measured the two mesas' conductances in two configurations, as indicated in Fig. 1(b). In configuration I, $\mathbf{B}_{\text{plane}}$ was parallel to face a . The samples

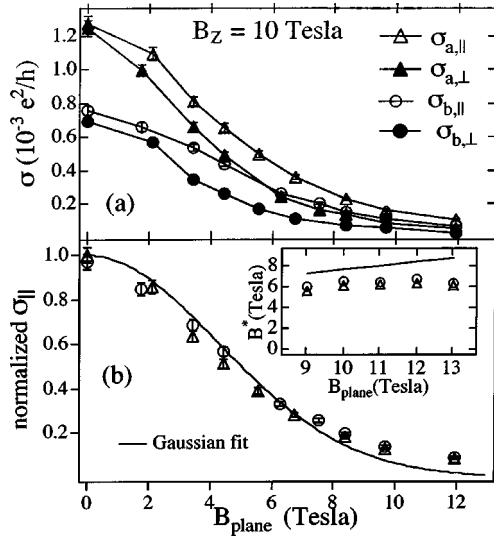


FIG. 2. Chiral sheath conductivities. (a) Conductivity on the two crystal faces as a function of in-plane magnetic field $\mathbf{B}_{\text{plane}}$, at a fixed $B_z = 10$ T, for the two measurement configurations. When $\mathbf{B}_{\text{plane}}$ is oriented perpendicular to a given mesa wall, the conductivity decrease is larger than when $\mathbf{B}_{\text{plane}}$ is parallel to the wall. (b) Dependence of σ_{\parallel} on B_{plane} at $B_z = 10$ T. Solid lines: Gaussian fits, which give the field scale B^* for the decay of interlayer tunneling. Inset: fitted B^* versus B_z . Solid lines are the prediction of Eq. (1).

were thermally cycled and remounted, rotated by 90° , for measurements in configuration II ($\mathbf{B}_{\text{plane}}$ parallel to face b).

Figure 1(d) plots the conductance G_1^I of mesa 1, measured in configuration I, versus B_z for a number of tilt angles. The subscript on G indexes the mesa and the superscript the measurement configuration. As shown, increasing the in-plane field by tilting the mesa reduces interlayer transport both within and between QH states. In configuration I the mesas' conductances in QH states are $G_1^I = 2(L\sigma_{a,\parallel} + W\sigma_{b,\perp})/H$ and $G_2^I = 2(W\sigma_{a,\parallel} + L\sigma_{b,\perp})/H$, while in configuration II, $G_1^{II} = 2(W\sigma_{b,\parallel} + L\sigma_{a,\perp})/H$ and $G_2^{II} = 2(L\sigma_{b,\parallel} + W\sigma_{a,\perp})/H$. We invert these expressions to obtain $\sigma_{a,\parallel}$, $\sigma_{a,\perp}$, $\sigma_{b,\parallel}$, and $\sigma_{b,\perp}$.

Figure 2(a) plots the conductivities of the chiral sheath on type a crystal faces (triangles) and on type b crystal faces (circles), as a function of B_{plane} at $B_z = 10$ T. Results at other B_z across the $\nu = 1$ QH state are similar. Open symbols show σ_{\parallel} and solid symbols show σ_{\perp} . The error bars indicate the reproducibility of different data sets taken at a given tilt angle from a day to a few weeks apart. Statistical errors in the measurements are much smaller.

Figure 2(a) shows that for both crystal faces, $\sigma_{\perp} < \sigma_{\parallel}$ for all fields. Apparently, $\mathbf{B}_{\text{plane}}$ is more effective at reducing the conductivity when it is perpendicular to the chiral sheath. Flux linked through the edge-state film then suppresses, rather than enhances, its conductivity, in contrast to conventional 2D systems.

We now use a simple model to attempt to separate the effects of the edge Lorentz force, which should affect only σ_{\perp} , from the decay in interlayer tunneling, which affects both σ_{\perp} and σ_{\parallel} . We assume that $\mathbf{B}_{\text{plane}}$ changes σ_{\parallel} through the reduction of t^2 , and that $\mathbf{B}_{\text{plane}}$ changes σ_{\perp} both through

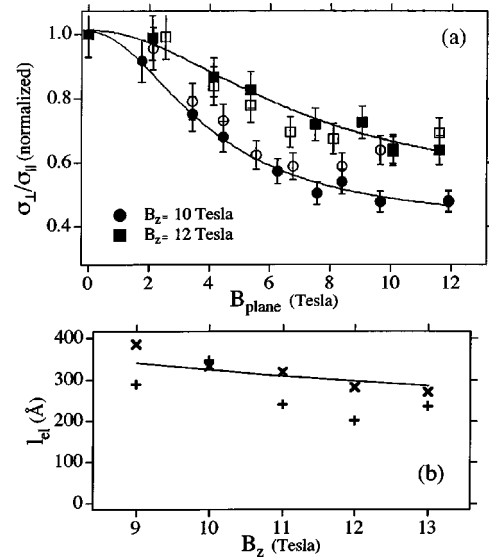


FIG. 3. Field dependence of $\sigma_{\perp}/\sigma_{\parallel}$, which shows the trajectory effect f_{\perp} produced by flux through the chiral sheath. (a) Ratios $\sigma_{b,\perp}/\sigma_{a,\parallel}$ (open symbols; configuration I) and $\sigma_{a,\perp}/\sigma_{b,\parallel}$ (solid symbols; configuration II) at $B_z = 10$ and 12 T. The ratios are normalized by their values at $B_{\text{plane}} = 0$ to factor out the difference in conductivity on type a and type b crystal faces. The solid lines show fits to Eq. (2). (b) Edge elastic scattering length l_{el} extracted from the fitted field scale B_0 . The plot symbols and (x) are results from configuration I (II). The solid line shows $4l_z$, for comparison. The difference in the fitted l_{el} for the two configurations gives a rough measure of the systematic errors in the analysis.

reduction of t and independently through the effect of the Lorentz force on edge trajectories. Then for a fixed value of B_z , $\sigma_{\parallel} \propto t^2(B_{\text{plane}})$ and $\sigma_{\perp} \propto t^2(B_{\text{plane}})f_{\perp}(B_{\text{plane}})$, respectively, where $f_{\perp}(B_{\text{plane}})$ describes the effect of flux through the chiral sheath. If the theory of Eq. (2) applies, $f_{\perp}(B_{\text{plane}}) \propto [1 + (B_{\text{plane}}/B_0)^2]^{-1}$. In principle, the B_{plane} dependence of t^2 and of f_{\perp} could differ on type a and b faces, but we find no evidence for this in the data: the ratios $\sigma_{a,\parallel}/\sigma_{b,\parallel}$ and $\sigma_{a,\perp}/\sigma_{b,\perp}$ are independent of B_{plane} , within experimental error.

Figure 2(b) shows the dependence of σ_{\parallel} on B_{plane} , which we take to represent the B_{plane} dependence of t^2 . The plot shows $\sigma_{a,\parallel}$ (triangles) and $\sigma_{b,\parallel}$ (circles), normalized by their $\theta = 0$ values, at $B_z = 10$ T. Results at other fields across the $\nu = 1$ QH state were similar. The solid line is a fit to Eq. (1), treating B^* as a fit parameter. As shown in the inset, the fitted B^* is ~ 70 – 80% of the expected value $B^* = 2B_z l_z/d$, where $l_z = (h/2\pi e B_z)^{1/2}$. The agreement between experiment and theory for bulk tunneling [Eq. (1)] is surprisingly good, since varying B_z may also change σ_{\parallel} through v_{edge} and l_{el} .

To determine the trajectory effect f_{\perp} of fields perpendicular to the chiral sheath, we examine the ratio $\sigma_{\perp}/\sigma_{\parallel}$. Figure 3(a) displays $\sigma_{\perp}/\sigma_{\parallel}$, normalized by its value at $\theta = 0$, for $B_z = 10$ T (circles) and for $B_z = 12$ T (squares). Open (solid) plot symbols are for configuration I (II). As shown, both configurations give similar results for the field dependence of

$\sigma_{\perp}/\sigma_{\parallel}$. For increasing $\mathbf{B}_{\text{plane}}$, the $\sigma_{\perp}/\sigma_{\parallel}$ ratios decay, with a larger field scale in $\mathbf{B}_{\text{plane}}$ at higher \mathbf{B}_z .

In Fig. 3(a), $\sigma_{\perp}/\sigma_{\parallel}$ does not appear to approach zero at large $\mathbf{B}_{\text{plane}}$, in disagreement with Eq. (2). SEM images of the mesas show etched walls that appear flat and smooth in the vertical direction, but that are somewhat corrugated laterally. Such corrugation would reduce orientation dependence by mixing the true σ_{\perp} and σ_{\parallel} in the estimated conductivities. This would have the effect of adding an offset to the nominal $\sigma_{\perp}/\sigma_{\parallel}$ ratio, so we take $\sigma_{\perp}/\sigma_{\parallel}$ to be the sum of a component insensitive to flux through the sheath, and a Drude term [Eq. (2)]:

$$\sigma_{\perp}/\sigma_{\parallel} = c_1 + c_2/[1 + (\mathbf{B}_{\text{plane}}/\mathbf{B}_0)^2]. \quad (4)$$

Walls with equal perpendicular and parallel areas to $\mathbf{B}_{\text{plane}}$, or incoherent transport, would yield $c_2=0$; while flat walls and full interlayer coherence imply $c_1=0$. The solid lines in Fig. 3(a) show examples of the fits of Eq. (4) to the data, which give $c_1/c_2 \sim 0.7$. The observed decay in $\sigma_{\perp}/\sigma_{\parallel}$ with increasing $\mathbf{B}_{\text{plane}}$ indicates that the samples are away from the incoherent limit, as is consistent with the observation of reproducible fluctuations¹ in G in QH states.

The fits of $\sigma_{a\perp}/\sigma_{b\parallel}$ and $\sigma_{b\perp}/\sigma_{a\parallel}$ to Eq. (4) give the field scale \mathbf{B}_0 for suppression of vertical transport by perpendicular $\mathbf{B}_{\text{plane}}$. Figure 3(b) plots the corresponding edge elastic scattering length, assuming $l_{\text{el}} = h/(edB_0)$ as in Eq. (2). As shown, l_{el} appears to decrease with increasing \mathbf{B}_z . We find $l_{\text{el}} \sim 4l_z$ [solid line in Fig. 3(b)], where $l_z = (h/2\pi eB_z)^{1/2}$ is the magnetic length associated with the vertical field B_z that establishes the QH state. The values of $l_{\text{el}} \sim 300 \text{ \AA}$ satisfy the inequality $l_{\text{el}} \gg l_z^2/d$ ($\sim 20 \text{ \AA}$ at 10 T), as required for validity of Eq. (2).⁷

We believe that the small value of l_{el} may reflect deviations from flatness of the sheath in the vertical direction, which would cause \mathbf{B}_z to link flux between edge states in adjacent layers and produce a relative phase shift that contributes to l_{el} . With $B_z \sim 10 \text{ T}$ across the $\nu=1$ QH state, a

small average displacement of $\sim 20 \text{ \AA}$ between adjacent edge states would produce a unit phase shift over distances in the chiral direction on the order of the fitted l_{el} . However, the model that leads to Eq. (2) considers impurity scattering at the edge to be the source of the dependence of $\sigma_{\perp}/\sigma_{\parallel}$ on $\mathbf{B}_{\text{plane}}$, rather than flux linked by surface roughness, and it is not obvious to us that the latter will yield the same behavior as predicted in Eq. (2). Regardless of the details of the model, our observation of field dependence in $\sigma_{\perp}/\sigma_{\parallel}$ provides information on the interlayer transport regime. Disorder and surface roughness will cause some degree of relative meander of edge states in adjacent layers, with a corresponding modulation in interlayer tunneling strength around the perimeter. If the meander is large enough, strong tunneling sites where adjacent, meandering edge states overlap will dominate transport. The data show that if such strong tunneling points do dominate, these sites must be close enough together that the flux the field links between them is well below a flux quantum. Otherwise, as discussed in Ref. 7, $\sigma_{\perp}/\sigma_{\parallel}$ would be independent of $\mathbf{B}_{\text{plane}}$.

In summary, the vertical conductivity data show that the effects of magnetic fields on the chiral sheath are qualitatively different than in ordinary 2D systems. We observe that the ratio $\sigma_{\perp}/\sigma_{\parallel}$ falls with increasing field strength. Within the model of Ref. 7, this effect arises from the suppression of σ_{\perp} by Lorentz forces on the chiral flow along the edge. In contrast, for typical isotropic conducting films without strong spin-orbit effects, $\sigma_{\perp}/\sigma_{\parallel}$ rises with increasing field strength due to the enhancement of σ_{\perp} by suppression of weak localization¹¹ and to relative field insensitivity of σ_{\parallel} . High in-plane fields applied to high quality two-dimensional electron gas systems can significantly affect their conductivity,¹⁰ but the effect that has been observed is a strong suppression of σ_{\parallel} , which would tend to cause $\sigma_{\perp}/\sigma_{\parallel}$ to rise with increasing field, rather than decay as we observe.

We acknowledge support from NSF-DMR 9700767 and NSF-DMR 0071956 and helpful discussion with J. T. Chalker.

¹D. P. Druist, P. J. Turley, E. G. Gwinn, K. D. Maranowski, and A. C. Gossard, Phys. Rev. Lett. **80**, 365 (1998).

²D. P. Druist, E. G. Gwinn, K. D. Maranowski, and A. C. Gossard, Physica E (Amsterdam) **6**, 619 (2000).

³B. Zhang, J. Brooks, Z. Wang, J. Simmons, J. Reno, N. Lumpkin, J. O'Brien, and R. Clark, Phys. Rev. B **60**, 8743 (1999); B. Zhang *et al.*, Physica B **258**, 279 (1998).

⁴M. Kawamura *et al.*, Physica B **298**, 48 (2001).

⁵L. Balents and M. P. A. Fisher, Phys. Rev. Lett. **76**, 2782 (1996).

⁶J. T. Chalker and A. Dohmen, Phys. Rev. Lett. **75**, 4496 (1995).

⁷J. T. Chalker and S. L. Sondhi, Phys. Rev. B **59**, 4999 (1999).

⁸J. Hu and A. H. MacDonald, Phys. Rev. B **46**, 12 554 (1992).

⁹D. P. Druist, E. G. Gwinn, K. D. Maranowski, and A. C. Gossard, Physica E **12**, 129 (2002).

¹⁰S. A. Vitkalov *et al.*, Phys. Rev. Lett. **85**, 2164 (2000).

¹¹P. A. Lee and T. V. Ramakrishnan, Rev. Mod. Phys. **57**, 287 (1985).